View metadata, citation and similar papers at core.ac.uk
brought to you by CORE
provided by DSpace@MIT

ANALYSIS OF HETEROGENEOUS OXYGEN EXCHANGE AND FUEL OXIDATION ON THE CATALYTIC SURFACE OF PEROVSKITE MEMBRANES

Jongsup Hong [a], Patrick Kirchen [b], Ahmed F. Ghoniem [a,*]

[a] *Department of Mechanical Engineering, Massachusetts Institute of Technology, 77 Massachusetts Avenue, Cambridge, MA 02139, USA*

[b] *Department of Mechanical Engineering, University of British Columbia, 2054-6250 Applied Science Lane, Vancouver BC, V6T 1Z4, CANADA*

Key Words: Perovskite membrane; Catalytic membrane reactor; Oxygen surface exchange; Surface reaction; Catalytic fuel conversion; Catalytic kinetics.

ABSTRACT

The catalytic kinetics of oxygen surface exchange and fuel oxidation for a perovskite membrane is investigated in terms of the thermodynamic state in the immediate vicinity of or on the membrane surface. Perovskite membranes have been shown to exhibit both oxygen perm-selectivity and catalytic activity for hydrocarbon conversion. A fundamental description of their catalytic surface reactions is needed. In this study, we infer the kinetic parameters for heterogeneous oxygen surface exchange and catalytic fuel conversion reactions, based on permeation rate measurements and a spatially resolved physical model that incorporates detailed chemical kinetics and transport in the gas-phase. The conservation equations for surface and bulk species are coupled with those of the gas-phase species through the species production rates from surface reactions. It is shown that oxygen surface exchange is limited by dissociative/associative adsorption/desorption of oxygen molecules onto/from the membrane surface. On the sweep side, while the catalytic conversion of methane to methyl radical governs the overall surface reactions at high temperature, carbon monoxide oxidation on the membrane surface is dominant at low temperature. Given the sweep side conditions considered in ITM reactor experiments, gas-phase reactions also play an important role, indicating the significance of investigating both homogeneous and heterogeneous chemistry and their coupling when examining the results. We show that the local thermodynamic state at the membrane surface should be considered when constructing and examining models of oxygen permeation and heterogeneous chemistry.

---

* Corresponding author. Tel.: +1 617 253 2295; Fax: +1 617 253 5981
Email address: ghoniem@mit.edu (Ahmed F. Ghoniem)

1. INTRODUCTION

Perovskite membranes have been shown to exhibit not only oxygen perm-selectivity suitable for air separation [1], but also catalytic activity for hydrocarbon conversion [2]. Possessing mixed ionic and electronic conductivity, dense perovskite membranes or ion-transport membranes (ITM) are able to selectively permeate oxygen ions from the air (feed) side to the sweep (permeate) side, driven by the oxygen chemical potential gradient at high temperature. In addition, these membranes have been shown to act as hydrocarbon conversion catalysts [2, 3], which, coupled with oxygen permeation, could enable their use as membrane reactors, in which fuel conversion reactions take place on the sweep side in the absence of nitrogen. Multiple applications have been proposed [4]. Methane is typically used as a feedstock, and its conversion to higher hydrocarbons, i.e., oxidative coupling of methane [5-8], syngas via partial oxidation of methane [9-11], or complete oxidation to carbon dioxide and water, i.e., oxy-fuel combustion [12] has been investigated. In spite of these promising applications, little is known about the fundamentals of catalytic fuel conversion processes on the sweep side of an ITM and their interactions with oxygen permeation and the homogeneous-phase flow, transport and chemical reactions.

Examining the fundamentals of catalytic fuel conversion and how they couple with oxygen permeation and gas-phase reactions require detailed and complex models. ITM reactors supply pure oxygen through the membrane to the sweep side where a fuel is introduced and oxidized. The coupling between catalytic fuel conversion and oxygen permeation is significant [6]. Since the oxygen permeation rate is not known a priori but rather depends on the local thermodynamic state (the oxygen concentration on both sides of the membrane and its temperature), fuel conversion on the membrane surface may change the oxygen permeation, and vice versa. Moreover, perovskite membranes typically require temperatures above 800 °C to enable oxygen permeation [1], and they have been employed at 800 ~ 1000 °C when fuel conversion is considered [4]. At high temperature, the fuel conversion may take place through homogeneous as well as catalytic surface reactions and ultimately impact the extent of fuel conversion and product selectivity [13]. Therefore, to examine the fundamental interactions and control fuel conversion and oxygen permeation, a detailed analysis that accounts for the coupling of oxygen permeation, gas-phase flow and transport, and homogeneous and heterogeneous chemistry in terms of the local thermodynamic state on both sides of the membrane surface is needed. The heterogeneous chemistry on the ITM surface has so far not been described in detail.

Akin and Lin [14] assumed different permeation mechanisms and two limiting oxidation kinetics: either extremely fast reaction or no conversion. Using a simple reactor model such as a continuously stirred tank reactor (CSTR), they examined how the oxidation reaction rates, the reducing gas flow rate and the feed-side oxygen partial pressure influence the oxygen permeation rate. Based on the same CSTR model, Rui et al. [15] investigated the effect of the finite chemical kinetic rates on the oxygen permeation rate. Results from these studies have shown that chemical reactions and their kinetic rates have substantial influence on the oxygen permeation. These models considered a CSTR and assumed arbitrary reaction rates. Wang and Lin [16] estimated catalytic kinetic parameters assuming that perovskite membranes behave catalytically in a way similar to Li/MgO membranes and applied them to the CSTR model, while Tan et al. [12] used the kinetic parameters of perovskite membranes for a plug flow reactor model. Although some modeling studies have also been performed on membrane reactors for syngas production [17-20], these considered additional catalysts mounted on the membrane surface, and hence the results are not representative of the catalytic activities of the perovskite membrane itself. Modeling studies conducted so far have not related the heterogeneous chemistry for perovskite membranes to the local thermodynamic state, and have not resolved its coupling with the oxygen permeation and gas-phase transport and reactions in detail.

In our previous studies, we examined the homogeneous-phase chemical reactions taking place on the sweep side of the perovskite membrane and their influences on oxygen permeation and fuel conversion using a spatially resolved physical model. The model incorporated detailed gas-phase chemical kinetics and transport and was used to parameterize the oxygen permeation rate expression in terms of the gas-phase oxygen concentrations in the immediate vicinity of the membrane [21], as well as to characterize the homogeneous-phase reaction environment on the sweep side of an ITM [22]. A parametric study of key operating parameters was conducted to investigate the interactions between oxygen permeation and homogeneous fuel oxidation reactions [13]. The results from these investigations showed that, at the conditions relevant to high temperature membrane reactor operation, the local thermodynamic state in the immediate vicinity of the membrane should be considered when examining the oxygen permeation rate and the extent of fuel conversion. Furthermore, it was argued that heterogeneous chemistry may contribute to oxygen permeation, fuel conversion and product selectivity. For that purpose, an analysis using a model that incorporates both homogeneous and heterogeneous chemistry coupled with oxygen permeation in terms of the local thermodynamic state is proposed here.

In this study, we develop a heterogeneous kinetic mechanism for a perovskite membrane. Our computational model builds on our previous work [13, 21, 22]. To develop the heterogeneous chemistry for $La_{0.6}Sr_{0.4}Co_{0.2}Fe_{0.8}O_{3-\delta}$ (LSCF) membranes, the model incorporates conservation equations for the concentrations of surface and bulk (solid-state), i.e., incorporated into the lattice, species. We first estimate the kinetic parameters for oxygen surface exchange processes using experimentally measured mean oxygen permeation rates [23] in which an inert gas is used on the sweep side. Next, incorporating these oxygen surface exchange kinetic parameters, we estimate the kinetic parameters for catalytic surface fuel reactions by comparing the predicted permeation rates to measurements using methane [6, 7], carbon monoxide [24] or hydrogen [25] as the reactive sweep gas. In Section 2, the numerical model employed in this study is described. Section 3 summarizes the methodology used to develop heterogeneous chemistry and to estimate the kinetic parameters for oxygen surface exchange and catalytic fuel conversion. In Section 4, the importance of the local thermodynamic state when constructing and examining heterogeneous chemistry is discussed.

2. MODEL FORMULATION

The heterogeneous chemistry for a high temperature ion transport membrane surface is now developed. In our previous study [21], we formulated a homogeneous-phase physical model for a planar, finite-gap stagnation-flow configuration (see Figure 1) that couples the gas-phase flow, transport and chemical reactions, and oxygen permeation flux and heat flux across the membrane. In this study, this model is augmented to incorporate the heterogeneous chemistry. Note that detailed chemistry and transport in both homogeneous and heterogeneous phases should be considered to examine the fundamentals of ITM reactors [14, 15]. This is implemented by selecting the self-similar stagnation-flow configuration to keep the computational cost at a manageable level. This self-similar solution captures most of the features of typical laboratory scale reactors used to measure the permeation flux, while allowing sufficiently detailed analysis of the thermo-chemical-transport processes close to the membrane surface, without requiring a comprehensive multi-dimensional characterization.

2.1. Species Conservation Equations and Their Coupling

The overall model, including the time dependent continuity, momentum, energy and species conservation equations, has been described in detail in [21]. Here the species conservation equation is shown for illustration. To account

for surface reactions and the role of catalytic chemistry, the concentrations of surface and bulk species are considered as solution variables. Figure 2 shows how the overall field is divided into three domains and the species that belong to each domain. This includes two volumetric domains, which are the gaseous and bulk (solid) domains, and one interfacial domain between them. The transport-chemistry interaction in each domain is modeled using the appropriate form of the differential equations, while surface reactions are used to connect them.

The species concentration in the gaseous domain is governed by the following equation:

$$\rho\frac{\partial Y_k}{\partial t}+V\frac{\partial Y_k}{\partial y}+\frac{\partial j_k^g}{\partial y}-\dot{\omega}_k W_k=0 \qquad \text{: Gas-phase species} \qquad \text{(Eq.1)}$$

$$\text{where, } j_k^g=-\rho D_{km}\left(\frac{\partial Y_k}{\partial y}+\frac{Y_k}{\bar{W}}\frac{\partial \bar{W}}{\partial y}\right)-\frac{D_k^T}{T}\frac{\partial T}{\partial y}$$

where ρ is the gas-phase density [kg/m^3]; Y_k is the mass fraction of gas-phase species k; V is the convective mass flux [kg/m^2/s]; j_k^g is the diffusive mass flux of gas-phase species k [kg/m^2/s]; $\dot{\omega}_k$ is the molar production rate of gas-phase species k through homogeneous chemistry [kmol/m^3/s]; W_k is the molecular weight of gas-phase species k [kg/kmol]; D_{km} is the mixture-averaged diffusion coefficient [m^2/s]; D_k^T is the thermal diffusion (Soret effect) coefficient [kg/m/s]; $\bar{W}$ is the mixture molecular weight [kg/kmol]; T is the gas temperature [K]. A detailed chemical kinetic mechanism (GRI-Mech 3.0 [26]) is employed for homogeneous-phase chemical reactions. Cantera [27] along with NASA polynomials is used to integrate multi-step chemical reactions and evaluate thermodynamic and transport properties. The gaseous domains are connected with the surface domains by heterogeneous chemical reactions and other boundary conditions. At steady state, the gas-phase species produced or consumed by surface reactions should be balanced with convective and diffusive mass fluxes into or from the gaseous domain, respectively. The mass-flux-matching boundary conditions are described as follows:

$$V_{mem}=\sum_{k=1}^{N_g}\dot{s}_k W_k \qquad \text{(Eq.2)}$$

$$j^{g}_{k,mem} + Y_{k,mem} V_{mem} = \dot{s}_k W_k \qquad (k = 1, ..., N_g) \tag{Eq.3}$$

where V_{mem} is the convective mass flux at the membrane surface [kg/m^2/s]; $j^{g}_{k,mem}$ is the diffusive mass flux at the membrane surface [kg/m^2/s]; $Y_{k,mem}$ is the mass fraction of gas-phase species *k* at the membrane surface boundary; $\dot{s}_k$ is the molar surface production rate of species *k* through heterogeneous chemistry [kmol/m^2/s]; N_g is the number of gas-phase species. These two matching conditions, Eq.2 and Eq.3, describe the transition from gas-phase to surface species.

Moreover, we need to relate gas-phase and surface species to bulk (solid-state) species. The bulk species concentration in the direction of the membrane thickness is governed by bulk diffusion, j^{b}_{k} (see Figure 2). The control volume approach is used to relate the volumetric bulk domain with the interface domain. The species concentration in the bulk domain is resolved by considering a small control volume $d\forall$ adjacent to the surface [28, 29]:

$$\int \hat{\rho}_{mem} \frac{\partial C_k}{\partial t} d\forall - \int \dot{s}_k \, dA + \int j^{b}_{k} \, dA = 0 \qquad \text{: Bulk species} \tag{Eq.4}$$

where $\hat{\rho}_{mem}$ is the molar density of the membrane [kmol/m^3]; C_k is the molar fraction of bulk species *k*; j^{b}_{k} is the diffusive flux of bulk species *k* through the membrane [kmol/m^2/s]. Per the discussion in Section 3.1, we consider two bulk species: the oxygen vacancy and lattice oxygen ion. It has been argued that the oxygen vacancy is a mobile charged-species whose transport within the membrane represents the overall bulk diffusion process [4] and can be described by the following expression,

$$j^{b}_{V_O^{\bullet\bullet}} = -\hat{\rho}_{mem} D_{V_O^{\bullet\bullet}} \frac{\partial C_{V_O^{\bullet\bullet}}}{\partial y} \tag{Eq.5}$$

where $D_{V_O^{\bullet\bullet}}$ is the diffusivity of the oxygen vacancy inside the membrane [m^2/s]. At steady state, assuming the constant value for $D_{V_O^{\bullet\bullet}}$, this equation, Eq.5, yields,

$$j^b_{V_O^{\bullet\bullet}} = -\frac{\hat{\rho}_{mem} D_{V_O^{\bullet\bullet}}}{L}\left(C_{V_O^{\bullet\bullet},sweep} - C_{V_O^{\bullet\bullet},air}\right) \quad \text{(Eq.6)}$$

where L is the membrane thickness [m]; $C_{V_O^{\bullet\bullet},sweep}$ and $C_{V_O^{\bullet\bullet},air}$ are the molar fractions of the oxygen vacancy on the sweep and air side surfaces of the membrane, respectively. The derivation of Eq.5 was discussed in [21]. The diffusivity of the oxygen vacancy for an LSCF membrane was found in [21, 23] and depends on the membrane temperature and crystalline structure. The flux of the oxygen vacancy is counter-balanced by the movement of bulk oxygen ions in the opposite direction. At isothermal, steady state conditions, and with small differences in the oxygen concentration across the membrane, the diffusivity of the oxygen vacancy can be assumed constant. Moreover, we assume no spatial gradients of bulk species along the membrane (x-direction in Figure 1). Thus, at steady state, the bulk species produced or consumed by surface reactions must be balanced with a diffusive flux into or from the bulk domain, and Eq.4 results in the flux-matching condition,

$$\dot{s}_k = j^b_k \quad (k = 1, ..., N_b) \quad \text{(Eq.7)}$$

where N_b is the number of bulk species. This condition describes the transition from surface to bulk species.

The species conservation within the interface domain is accounted for by surface reactions without species transport or mass fluxes. The following describes the surface species concentration in the surface domain:

$$\Gamma \frac{\partial Z_k}{\partial t} - \dot{s}_k = 0 \quad \text{: Surface species} \quad \text{(Eq.8)}$$

where Γ is the total available surface site density [kmol/m^2]; Z_k is the surface site occupancy of surface species *k* (i.e., the molar fraction of available surface sites covered by surface species *k*). Per the discussion in Section 3.1, we consider two

surface species: the vacant surface site and adsorbed surface oxygen anion. At steady state, the surface species conservation equation, Eq.8, yields the condition that the net production or consumption of surface species is zero,

$$\dot{s}_k = 0 \qquad (k = 1,..., N_s) \tag{Eq.9}$$

where N_s is the number of surface species.

The heterogeneous kinetic mechanism developed in this study is based on the species concentration at and immediately below the surface domain and used for the coupling conditions between the three domains. The spatially resolved physical model (the model) enables an estimation of the kinetic parameters for surface reactions based on the local thermodynamic state. In addition, as shown in Eq.2 to Eq.4 and Eq.7 to Eq.9, the species molar production rates through surface reactions relate the bulk domains and the interface domain. The production and consumption of all gas-phase, surface and bulk species from each surface reaction are considered in connecting these domains.

2.2. Thermal Energy Balance of the Membrane

The thermal energy balance of the membrane is attributed to the conductive, convective and diffusive heat transfer with the gaseous domain (i.e., Q''_{air} and Q''_{sweep} [W/m^2]) and the heat release from surface reactions as well as the thermal radiation between the membrane and the reactor walls, which is expressed as follows:

$$Q''_{sweep} - Q''_{air} - 2\sigma\varepsilon_{mem}\left(T_{mem}^4 - T_\infty^4\right) - \sum_{k=1}^{N_s+N_b} \hat{h}_k \, \dot{s}_k = 0 \tag{Eq.10}$$

$$\text{where, } Q''_{air} = -\lambda\nabla T + \sum_{k=1}^{N_g}\left(j_{k,mem}^g + Y_{k,mem}V_{mem}\right)\hat{h}_k$$

$$Q''_{sweep} = \lambda\nabla T - \sum_{k=1}^{N_g}\left(j_{k,mem}^g + Y_{k,mem}V_{mem}\right)\hat{h}_k$$

where σ is the Stefan-Boltzmann constant [W/m^2/K^4]; ε_{mem} is the emissivity of the membrane; T_{mem} and T_{∞} are the membrane and surrounding wall temperature, respectively [K]; $\hat{h}_k$ is the molar enthalpy of species *k* [J/kmol]; λ is the mixture thermal conductivity [W/m/K]. Thermodynamic properties of surface and bulk species on perovskites are obtained from [30], assuming that they are similar to those on YSZ. Note that since typical membranes are very thin [4], we assume that no temperature gradient exists inside the membrane (i.e., uniform membrane temperature). More modeling details are given in our previous study [21].

3. HETEROGENEOUS CHEMISTRY

To characterize the catalytic activity of a perovskite membrane and examine its coupling with oxygen permeation and gas-phase transport and reactions, a description of the heterogeneous chemistry is needed. This should account for two important types of kinetics: oxygen surface exchange on both sides of the membrane and catalytic fuel conversion on the sweep side. Oxygen is introduced into the reactor through the (catalytically active) membrane and the fuel in the sweep stream. Therefore, a heterogeneous kinetic mechanism must resolve catalytic fuel conversion, which is also coupled with oxygen permeation. To investigate oxygen surface exchange processes, we use permeation measurements obtained using an inert sweep gas [23] and our model for flow, transport and chemistry across the entire domain. The model, expanded to include the oxygen surface exchange kinetics, is then used to estimate the kinetic parameters for catalytic fuel conversion, using the experimental data acquired when a reactive gas is introduced into the sweep side of the membrane [6, 7, 24, 25]. The experimental conditions at which the measurements were carried out, including the air and sweep gas flow rates, the molar compositions, and temperature, are used as boundary conditions at the air and sweep gas inlets for the model. Given these inlet conditions, the kinetic parameters were manually adjusted in order to obtain the same permeation rates as measured experimentally.

3.1. Oxygen Surface Exchange Kinetics

3.1.1. Oxygen surface exchange mechanism

A multi-step oxygen permeation kinetic mechanism is considered, which accounts for a sequence of oxygen surface exchange processes. The overall incorporation/discharge processes are described by,

$$\frac{1}{2}O_2 + V_O^{\bullet\bullet} \leftrightarrow O_O^x + 2h^{\bullet} \quad \text{(Eq.11)}$$

where $V_O^{\bullet\bullet}$ is the oxygen vacancy; O_O^x is the lattice (bulk) oxygen ion (charge number = −2); $h^{\bullet}$ is the electron hole. This one step reaction has been widely used to model the overall surface exchange processes. However, when fuel conversion occurs on the membrane surface, this global reaction, Eq.11, may not accurately capture the surface reactions because the fuel conversion reactions might influence some of the intermediate oxygen surface exchange processes. As shown in Figure 3, it has been suggested that the global oxygen surface exchange reaction can be described by a sequence of five intermediate steps [31] summarized as follows (refer to Figure 3 for step numbers, (i) through (v)):

- **i.** adsorption/desorption of gas-phase oxygen molecules onto/from the membrane surface
- **ii.** dissociation/association of adsorbed oxygen molecules into/from oxygen atoms
- **iii.** electron transfer with the lattice to form singly-charged surface oxygen anions/oxygen atoms
- **iv.** incorporation into/discharge from the crystalline structure by filling/forming an oxygen vacancy
- **v.** electron transfer with the lattice to form fully-charged/singly-charged bulk oxygen anions

With respect to oxygen transport, step (i) connects the gaseous domain and the interface domain, while steps (ii) and (iii) take place within the interface domain. Step (iv) relates the interface to the bulk domain, whereas step (v) occurs wholly inside the bulk domain. Using an oxygen isotope exchange technique, Boukamp et al. demonstrated that the kinetics of these five intermediate processes can be approximated by two rate-limiting single-electron transfer reaction steps [32, 33]. The first is the dissociative/associative adsorption/desorption, Eq.12, accounting for steps (i) to (iii), while the second is the charge-transfer incorporation/discharge, Eq.13, describing steps (iv) and (v), as shown below,

$$O_2 + 2(s) \xleftrightarrow{k_{f,1}/k_{b,1}} 2O^-(s) + 2h^{\bullet} \quad \text{: Surface reaction 1} \quad \text{(Eq.12)}$$

$$O^-(s) + V_O^{\bullet\bullet} \xleftrightarrow{k_{f,2}/k_{b,2}} O_O^x + (s) + h^{\bullet} \quad \text{: Surface reaction 2} \quad \text{(Eq.13)}$$

where (s) is the vacant surface site on the membrane surface; $O^-(s)$ is the adsorbed singly-charged surface oxygen anion; $k_{f,i}$ and $k_{b,i}$ are the reaction rate constants of forward and backward reactions, respectively, of Eq.12 and Eq.13; the subscript number in the reaction rate constants is the corresponding reaction number. All reaction rate constants are assumed in an Arrhenius format, as shown below:

$$k = AT_{mem}^{n} \exp\left(\frac{-E_A}{RT_{mem}}\right) \quad \text{(Eq.14)}$$

where A is the pre-exponential factor; n is the temperature exponent; E_A is the activation energy [J/mol]; R is the universal gas constant [J/mol/K]. To model the two rate-limiting steps, the concentrations of two surface species, (s) and $O^-(s)$, and two bulk species, $V_O^{\bullet\bullet}$ and O_O^x, are introduced as thermodynamic state variables in the analysis. Note that typical perovskite membranes have a high electronic conductivity, and hence, at steady state, the concentration of electron holes is considered constant throughout the membrane and its impact on the surface exchange reaction rate is neglected. Then, the net reaction rates, $\dot{R}_i$ [kmol/m^2/s], of Eq.12 and Eq.13 are expressed as follows:

$$\dot{R}_1 = k_{f,1}\left(\frac{\rho Y_{O_2}}{W_{O_2}}\right)\left(\Gamma Z_{(s)}\right)^2 - k_{b,1}\left(\Gamma Z_{O^-(s)}\right)^2 \quad \text{(Eq.15)}$$

$$\dot{R}_2 = k_{f,2}\left(\Gamma Z_{O^-(s)}\right)\left(\hat{\rho}_{mem} C_{V_O^{\bullet\bullet}}\right) - k_{b,2}\left(\hat{\rho}_{mem} C_{O_O^x}\right)\left(\Gamma Z_{(s)}\right) \quad \text{(Eq.16)}$$

Summing up these two reaction rates, we obtain the molar production rate of each species participating in the oxygen surface exchange reactions:

$$\dot{s}_k = \sum_{i=1}^{N_R} \nu_{k,i}\, \dot{R}_i \quad \text{(Eq.17)}$$

where N_R is the number of surface reactions; the subscript *i* is the reaction number; $\nu_{k,i}$ is the stoichiometric coefficient of species *k* in the reaction *i*. Note that Y_k, C_k and Z_k shown in Eq.15 and Eq.16 are the local species concentration in the gas-phase, in the bulk-phase, and on the membrane surface (i.e., interface domain), respectively. Thus, the reaction rate constants, $k_{f,i}$ and $k_{b,i}$, should be determined in terms of these local thermodynamic state variables, as will be evident in Section 4.

3.1.2. Estimation of kinetics rate parameters

The oxygen surface exchange kinetic parameters were estimated using the model, the surface kinetics model and the experimentally measured oxygen permeation rates. Using the LSCF membrane with an inert sweep gas, Xu and Thomson measured the oxygen permeation rates in a typical disc-type stagnation-flow permeation apparatus [23]. We use their data to estimate the kinetic parameters in Eq.15 and Eq.16. Note that each surface reaction, Eq.12 and Eq.13, needs forward and backward reaction rate constants, k_f and k_b, since the equilibrium constant is not known. That is, twelve parameters must be evaluated (refer to Eq.14). First, the sensitivity of each reaction to the temperature was examined by changing its activation energy, E_A, and temperature exponent, n. The activation energies and temperature exponents of the four reactions were adjusted simultaneously until we achieved the same temperature dependency of the predicted permeation rates as that of the measurements. Second, the four pre-exponential factors were varied to obtain the same absolute oxygen permeation rates as the experimentally measured values. In this estimation process, the initial values for the oxygen surface exchange kinetic parameters were obtained from solid oxide fuel cell studies [30, 34, 35]. The estimated values of these twelve oxygen surface exchange kinetic parameters are shown in Table 1.

As shown in Figure 4(a), the estimated oxygen surface exchange kinetic parameters result in an oxygen permeation rate that matches the measurements very well. The oxygen surface exchange kinetic parameters are also implemented at the sweep side of the membrane in cases when a reactive sweep gas is introduced. The reactive sweep gas conditions refer to [22], which include a methane concentration of 6% on a molar basis with the remainder being carbon dioxide, a sweep gas inlet temperature of 1300 K and a sweep gas flow rate of 4.39×10^{-4} m^3/s. At these conditions, it has been shown that reactants are mostly oxidized through gas-phase reactions and hardly reach the membrane surface, limiting

the role of catalytic fuel conversion. As shown in Figure 4(b), the predicted temperatures and heat release rates are in very good agreement with those reported in [22].

Figure 5 shows the oxygen surface exchange reaction rates for LSCF estimated by here using our model along with those for $(Y_2O_3)_{0.08}(ZrO_2)_{0.92}$ (YSZ), $La_2NiO_{4+\delta}$ (LNO) and $Ba_{0.5}Sr_{0.5}Co_{0.8}Fe_{0.2}O_{3-\delta}$ (BSCF) measured experimentally by Bouwmeester et al. [36]. The reaction rates calculated using the estimated kinetic parameters for LSCF fall in between those of YSZ and LNO. In all cases, the overall oxygen surface exchange processes are limited by the dissociative/associative adsorption/desorption, Eq.12 (R_1 in Figure 5). This is consistent with the results by Bouwmeester et al., in which they measured the reaction rates of Eq.12 and Eq.13 for YSZ, LNO and BSCF using a pulse isotopic exchange technique and showed that the dissociative/associative adsorption/desorption was rate-limiting. In addition, it is shown that oxygen surface exchange reactions estimated numerically for LSCF membrane are slower than those on LNO and BSCF, and faster than those on YSZ.

3.2. Catalytic Fuel Conversion Kinetics

Perovskite membranes have been proposed for fuel conversion applications such as oxy-fuel combustion and oxidative coupling of methane and have been shown to have some catalytic activity towards hydrocarbon conversion [2]. Although they have also been employed for syngas production, the product selectivity for syngas is very low without an additional catalyst mounted on the membrane surface [10]. The catalytic activity of perovskites for syngas production is not as strong as typical fuel conversion catalysts such as Nickel, Rhodium or Platinum, and the extent of fuel conversion from these membrane reactors is low [4]. In addition, the product selectivity is difficult to control when homogeneous chemistry plays a role and influences the final products. To control the fuel conversion and product selectivity effectively, the catalytic fuel conversion processes in a membrane reactor should be investigated further.

So far, the reaction mechanisms on a perovskite membrane surface have not been identified, and available measurements are not sufficient to formulate detailed surface reaction models. In light of this, we start with a set of global surface reactions for catalytic conversion of methane, carbon monoxide and hydrogen. The reaction rate parameters for catalytic fuel conversion are estimated by using the model described so far and experimentally measured permeation rates with methane [6, 7], carbon monoxide [24] or hydrogen [25] components in the sweep gas. Among the measured fuel

conversion, product selectivity and permeation rate, the oxygen permeation rates are most reliable, as the other two are more sensitive to gas-phase reactions and reactor geometries. Note that homogeneous chemistry is also implemented during the estimation of catalytic fuel conversion kinetic parameters in order to account for the possible influence of gas-phase reactions on the oxygen permeation and fuel conversion processes, as has been noted in [13, 22].

3.2.1. CH_4 catalytic decomposition

Experimental work has suggested that methane is catalytically converted in an ITM reactor, including the oxidative coupling pathway that produces ethane or ethylene [5-8]. The surface reactions of oxygen ions with methane yield C_2 hydrocarbons while inhibiting the formation of CO_x through the homogeneous-phase chemical reactions by reducing the availability of gas-phase oxygen [4]. It has been shown that a C_2H_6/O_2 co-feed reactor with no catalyst results in higher CO_x yields than when an LSCF surface is placed in the reactor [6]. This implies that the production of CO_x takes place in the homogeneous phase and that LSCF can suppress the production of CO_x by acting as a methane oxidative coupling catalyst. It should be noted, however, that this study was carried out under fuel rich conditions and this conclusion may not necessarily hold true for fuel/oxygen ratios closer to the stoichiometric ratio. On the other hand, Tan et al. [12] proposed that methane oxidation to carbon dioxide is also catalytically supported. However, they used a co-feed fixed bed reactor packed with granular LSCF, and hence their measurements are not representative of ITM reactors. To elucidate if perovskites can act as an oxidative coupling of methane catalyst or an oxidation catalyst, measurements such as product concentrations in the vicinity of the membrane are needed. Since they are not available, this study assumes that perovskites can contribute to the catalytic conversion of methane to methyl radical [16].

Most researchers agree that two successive steps can describe the overall oxidative coupling processes [16], although the detailed conversion mechanism for methane on the ITM surface is still not resolved:

- **i.** adsorption of methane, its conversion to methyl radicals by an oxygen ion on the membrane surface and the desorption of methyl radicals to the gas-phase
- **ii.** association of two methyl radical molecules in the gas-phase to form ethane or ethylene

With respect to step (i), Wang and Lin [16] proposed the following reaction,

$$2CH_4 + O_O^x \xrightarrow{k_{f,3}} 2CH_3 + H_2O + V_O^{\bullet\bullet} \quad \text{: Surface reaction 3} \qquad \text{(Eq.18)}$$

The methyl radicals produced from this reaction can be oxidized or combined to form higher hydrocarbons such as ethane in the gas-phase (step (ii)), which is resolved by detailed homogeneous chemistry implemented in our numerical model. The reaction rate of Eq.18 is expressed as,

$$\dot{R}_3 = k_{f,3}\left(\frac{\rho Y_{CH_4}}{W_{CH_4}}\right)^2 \left(\hat{\rho}_{mem} C_{O_O^x}\right) \qquad \text{(Eq.19)}$$

The activation energy of $k_{f,3}$ was evaluated by ten Elshof et al. [7] using their LSCF membrane reactor. To obtain the pre-exponential factor of $k_{f,3}$, we use the model and the experimental measurements of the oxygen permeation rates by Xu and Thomson [6] with methane in the sweep gas mixture. The estimated value of the parameter is shown in Table 1 for a temperature range of 1073K to 1223K and methane concentrations 25% to 100% on a molar basis. Since the kinetic parameters for the methane decomposition reaction obtained in this study are based on an ITM reactor experiment, they are more representative of the membrane catalytic activity than the values previously estimated [16], in which it was assumed that perovskite membranes behave catalytically in a way similar to Li/MgO membranes leading to a significantly lower activation energy.

During the parameterization of the catalytic CH_4 conversion reaction using the overall model, the homogeneous-phase chemical reactions were found to be relevant only near the membrane surface. Figure 6 shows the gas-phase molar production rates of methane, methyl radical, ethylene and ethane as estimated by the model incorporating the heterogeneous methane decomposition, given the sweep side conditions considered in the experiment. These are negligible in most of the gaseous domain on the sweep side, with the exception of the region approximately 1 mm from the membrane. Since the operating temperature, 1098 K, considered in the experiment is well below the ignition temperature for the onset of homogeneous chemistry (approximately 1200 K [13]), the effect of gas-phase reactions was suppressed. In the immediate vicinity of the membrane, the methyl radicals produced from the surface reaction, Eq.18, are combined in the gas-phase to

form ethylene and ethane, indicating the oxidative coupling of methane. In addition, when this ethane reacts further with the methyl radicals produced from heterogeneous chemistry, the formation of methane in the gas-phase is favored through the following reactions,

$$CH_3 + C_2H_6 \leftrightarrow C_2H_5 + CH_4 \qquad \text{(Eq.20)}$$

This effect reduces the extent of the overall CH_4 conversion, even if the conversion of methane is catalytically supported at the membrane surface. We conclude that the interactions between homogeneous and heterogeneous chemistry are important and should be considered in the analysis of fuel conversion processes in ITM reactors.

3.2.2. CO surface oxidation

van Hassel et al. [37] and ten Elshof et al. [24] demonstrated that the oxygen permeation rates increase when introducing carbon monoxide in the sweep side. They also showed that the oxygen permeation flux is raised with an increase of the carbon monoxide concentration in the sweep stream, arguing that the catalytic oxidation of carbon monoxide with oxygen on the membrane surface may contribute to the enhancement of the oxygen permeation rate. In addition, it has been shown that carbon monoxide produced from methane in the gas-phase reactions can reach the membrane surface when the gas-phase reaction zone approaches the membrane [13]. Therefore, the following carbon monoxide oxidation reaction [24, 37] should be included in the development of heterogeneous chemistry,

$$CO + O_O^x \xrightarrow{k_{f,4}} CO_2 + V_O^{\bullet\bullet} \qquad \text{: Surface reaction 4} \qquad \text{(Eq.21)}$$

The catalytic oxidation of carbon monoxide consumes the oxygen directly on the membrane surface, which enhances oxygen permeation. The reaction rate of Eq.21 is expressed as,

$$\dot{R}_4 = k_{f,4}\left(\frac{\rho Y_{CO}}{W_{CO}}\right)\left(\hat{\rho}_{mem} C_{O_O^x}\right) \qquad \text{(Eq.22)}$$

The activation energy of $k_{f,4}$ was evaluated by ten Elshof et al. [24] using their LSF membrane reactor. Assuming that LSCF membranes show similar catalytic behavior to that of the LSF membrane, we use the same value of the activation energy. To obtain the pre-exponential factor of $k_{f,4}$, we use the model and the experimentally measured oxygen permeation rates by ten Elshof et al., introducing carbon monoxide to the sweep side. The estimated value of the parameter is shown in Table 1 for a temperature range of 1173K to 1323K and carbon monoxide concentrations of 5% to 25% on a molar basis.

During the estimation of the kinetic parameters for carbon monoxide catalytic oxidation, the effect of the homogeneous chemistry on CO oxidation and oxygen permeation were found to be negligible. Figure 7 shows the gas-phase molar production rates of carbon monoxide and oxygen as estimated by the model incorporating the heterogeneous CO oxidation, given the sweep side conditions considered in the experiment. These are negligible throughout the gaseous domain on the sweep side, indicating the suppression of the homogeneous-phase reactions. This can be attributed to the absence of the hydroxyl radical which is required to oxidize carbon monoxide in the gas-phase [22]. Since hydrogen-containing species was not introduced in the sweep stream, the hydroxyl radical could not be formed or contribute to carbon monoxide oxidation in the gas-phase. In cases when methane is added to the sweep stream, it will provide the hydroxyl radical, and homogeneous oxidation will be accelerated. The relative roles of both depend on the condition and will be investigated in a future study.

3.2.3. H_2 surface oxidation

Perovskite membranes may contribute to the catalytic oxidation of hydrogen. Tan et al. [25] showed evidence that the oxygen permeation flux is raised with an increase of the hydrogen concentration in the sweep stream, and a large amount of water is produced due to the reactions. Furthermore, Hong et al. [13] showed that hydrogen produced from methane in the gas-phase reactions can reach the membrane surface when the gas-phase reaction zone is established in the vicinity of the membrane. We therefore propose to use the following oxidation reaction to account for the perovskite membrane catalytic activity for hydrogen oxidation, when constructing heterogeneous chemistry,

$$H_2 + O_O^x \xrightarrow{k_{f,5}} H_2O + V_O^{\bullet\bullet} \qquad \text{: Surface reaction 5} \qquad \text{(Eq.23)}$$

The catalytic oxidation of hydrogen consumes the oxygen directly on the membrane surface, increasing the oxygen permeation rate. The reaction rate of Eq.23 is expressed as,

$$\dot{R}_5 = k_{f,5}\left(\frac{\rho Y_{H_2}}{W_{H_2}}\right)\left(\hat{\rho}_{mem} C_{O_O^x}\right) \qquad \text{(Eq.24)}$$

To obtain the activation energy, exponent for temperature and pre-exponential factor of $k_{f,5}$, we use the model and the experimentally measured oxygen permeation rates by Tan et al. [25] introducing hydrogen into the sweep side. They use the LSF membrane reactor in their experiments. Assuming that LSCF membranes show similar catalytic activity for hydrogen oxidation to that of the LSF membrane, we use their measurements against which the kinetic parameters of Eq.23 are fitted. Since the oxygen permeation flux is predominantly dependent on the membrane temperature, the sensitivity of $k_{f,5}$ to the temperature is first examined. The activation energy and temperature exponent are varied simultaneously until achieving the same temperature dependency of the predicted permeation rates as that of the measurements. Then, the pre-exponential factor is adjusted to obtain the same oxygen permeation rates as those measured by Tan et al. The estimation of the kinetics parameters is summarized in Table 1 for a temperature range of 973K to 1273K and a hydrogen concentration of 30.8% on a molar basis.

In contrast to the other two cases in which methane or carbon monoxide was added to the sweep gas (refer to Section 3.2.1 and 3.2.2), a substantial impact of gas-phase reactions on hydrogen oxidation is demonstrated by the numerical simulations for the sweep side conditions considered in the experiment. Figure 8 shows the contribution of the catalytic surface reactions and the gas-phase reactions to hydrogen oxidation predicted by the model. Whereas gas-phase reactions are slow at low temperature, their role in hydrogen conversion is substantial and comparable to the catalytic reaction at high temperature. It has been typically assumed that the effect of homogeneous chemistry is negligible in comparison with that of heterogeneous chemistry within ITM reactors. However, as we show in this study, both homogeneous and heterogeneous chemistry should be taken into account.

3.2.4. Evaluation of catalytic fuel conversion kinetic parameters

The kinetic parameters for catalytic fuel conversion acquired in this analysis are based on the local thermodynamic state in the immediate vicinity of the membrane surface, on both sides and above and below the surface, as represented by the species concentrations in Eq.19, Eq.22 and Eq.24. The model accounts for these local concentrations. Mass transport and chemical reactions along the inlet and exit channels can change the species concentration and temperature significantly, which could lead to errors in the estimation of the kinetic parameters and the flux dependence on the operating conditions unless these effects are considered in the model. The model predicts this local thermodynamic state, and hence the kinetic parameters derived from it are more representative of what occurs on the membrane surface compared to parameters based on global values. As shown in Figure 9, the set of the reaction rate parameters for catalytic fuel conversion evaluated in this work provides estimates of the oxygen permeation rates that are in good agreement with measurements.

The catalytic activity for methane conversion and carbon monoxide oxidation predominantly govern the overall surface reactions on the membrane surface. Figure 10 shows the three reaction rate constants obtained in this study for CH_4 catalytic decomposition and CO and H_2 surface oxidation. The reaction rate constant of CH_4 catalytic decomposition is strongly dependent on temperature, whereas those of CO and H_2 surface oxidation are less sensitive to temperature. As a result, at low temperature (< 850 °C) CO surface oxidation governs the overall heterogeneous fuel conversion processes, while CH_4 catalytic decomposition plays a key role at high temperature (> 850 °C). Since ITM reactors operate at high temperature (i.e., above 900 °C), the CH_4 catalytic decomposition reaction may play an important role in fuel conversion and the enhancement of oxygen permeation. Furthermore, comparing Eq.19, Eq.22 and Eq.24, the CH_4 catalytic decomposition reaction is a second-order reaction with respect to the gas-phase species concentration, while the other two are first-order reactions. Therefore, given the same local gas-phase species concentration near the membrane, the catalytic CH_4 conversion reaction is more sensitive to the CH_4 concentration than other two reactions, and its effect may be more dominant in determining fuel conversion and oxygen permeation.

4. LOCAL THERMODYNAMIC STATE

Heterogeneous chemistry parameters evaluated in this work are based on the local thermodynamic state at the membrane estimated by the model. The variables defining this state are difficult to measure experimentally and, at this

point, can only be calculated using the model described here. When chemical reactions take place in the gas-phase and on the surface, the gas-phase species concentration and temperature measured outside the reactor can be substantially different from those in the immediate vicinity of the membrane. Thus, the model must be used to estimate the thermodynamic state and develop high fidelity heterogeneous chemistry. As shown in Figure 11 for the operating conditions considered for the estimation of the oxygen surface exchange parameters (Section 3.1), when the mass transfer in the gas-phase is substantial, the local thermodynamic state including species concentration and temperature varies significantly in the direction normal to the membrane. As the temperature is raised, the gas-phase oxygen concentration varies more extensively throughout the air and sweep gas domain. These spatial variations in the thermodynamic state have also been observed experimentally, using a specially designated experimental ITM reactor [38]. The operating temperature of ITM reactors is 900 °C or higher, and hence the local species concentrations near the membrane could be significantly different from those measured outside the reactor. Figure 12 shows the bulk oxygen ion concentration and oxygen partial pressure near the membrane on the sweep side, along with the sweep gas inlet conditions, for the same conditions considered when evaluating the oxygen surface exchange kinetic parameters (Section 3.1) and catalytic fuel conversion (Section 3.2). These results show that, when introducing a reactive sweep gas, the bulk oxygen ion concentration on the sweep side is smaller than that of an inert sweep gas because catalytic fuel conversion consumes oxygen ions directly on the membrane surface. As discussed in Section 3, catalytic fuel conversion competes for oxygen ions with oxygen discharge to the gas-phase, which, coupled with gas-phase reactions, results in a lower oxygen partial pressure in the vicinity of the membrane. The results show that substantial differences in these local species concentrations exist between two operating modes (i.e., inert sweep gas and reactive sweep gas), emphasizing the importance of considering the local thermodynamic state when investigating oxygen surface exchange and catalytic fuel conversion in the ITM reactor analysis.

5. CONCLUSIONS

Numerical simulations have been conducted to develop heterogeneous chemistry for a perovskite membrane in terms of the local thermodynamic state in the immediate neighborhood of the membrane and on its surface. In our previous study, we developed a physical model that resolves spatially the gas-phase flow, incorporates detailed homogeneous chemistry and accounts for oxygen permeation. In this paper, this model is revised to incorporate heterogeneous chemistry on the membrane surface. The surface and bulk species and their reactions are coupled with the local thermodynamic state

near the membrane in the gas phase. Using spatially averaged, i.e., reactor-level, measurements available in the literature, numerical simulations have been used to develop the heterogeneous chemistry that resolves both oxygen surface exchange and catalytic fuel conversion. A multi-step oxygen permeation mechanism is considered, which accounts for a sequence of bulk diffusion and surface exchange processes. While bulk diffusion is resolved by the charged-species transport, surface exchange processes are described by two rate-limiting reactions including dissociative/associative adsorption/desorption and charge-transfer incorporation/discharge. In addition, we consider three surface reactions for methane, carbon monoxide and hydrogen oxidation reactions to describe the catalytic activity of perovskite membranes.

Oxygen surface exchange and catalytic fuel conversion are resolved by the local thermodynamic state including gas-phase, surface and bulk species concentrations and temperature, and rate-limiting reactions are elucidated. The rates of heterogeneous reactions are expressed and evaluated in terms of the local species concentrations and temperature near the membrane or on the membrane surface. In agreement with previous experimental works, we show that oxygen surface exchange is limited by dissociative/associative adsorption/desorption of oxygen molecules onto/from the membrane surface. The estimated oxygen surface exchange reaction rates for LSCF fall in between the measured values for YSZ and LNO. In addition, while the catalytic conversion of methane to methyl radical governs the overall surface reactions at high temperature (> 850 °C), carbon monoxide oxidation on the membrane surface is dominant at lower temperature (< 850 °C). Given the typical ITM reactor operating conditions, gas-phase reactions also play an important role, highlighting the importance of both homogeneous and heterogeneous chemistry. We conclude that the local thermodynamic state should be accounted for when constructing and examining heterogeneous chemistry, though it should be noted that there are only very limited studies considering the local thermodynamic state experimentally or numerically and that more work is needed. In addition, many of the kinetic rate parameters for the heterogeneous reactions presented in this work were inferred from permeation measurements obtained without knowledge of the local thermodynamic state (which was inferred using the numerical model). Thus, in addition to spatially resolved experimental characterization of the thermodynamic state within an ITM reactor, there is a need for a more direct characterization of the surface processes. This includes the experimental identification of the most relevant catalytic fuel conversion reactions over all operating regimes of an ITM reactor, as well as the parameterization of the associated rate expressions. Future work will consider both these needs.

6. ACKNWOLEDGEMENTS

The authors would like to thank the King Fahd University of Petroleum and Minerals (KFUPM) in Dhahran, Saudi Arabia, for funding the research reported in this paper through the Center of Clean Water and Clean Energy at Massachusetts Institute of Technology and KFUPM. This work is also supported by King Abdullah University of Science and Technology grant number KSU-I1-010-01.

7. NOMENCLATURE

E_A	Activation energy [J/kmol]
$O^-(s)$	Adsorbed singly-charged surface oxygen anion
V	Convective mass flux [kg/m^2/s]
j_k^b	Diffusive flux of bulk species *k* through the membrane [kmol/m^2/s]
j_k^g	Diffusive mass flux of gas-phase species *k* [kg/m^2/s]
$D_{V_O^{\bullet\bullet}}$	Diffusivity of the oxygen vacancy [m^2/s]
$h^\bullet$	Electron hole
ε	Emissivity
ρ	Gas-phase density [kg/m^3]
O_O^x	Lattice (bulk) oxygen ion
Y_k	Mass fraction of gas-phase species *k*
L	Membrane thickness [m]
D_{km}	Mixture-averaged diffusion coefficient [m^2/s]
$\overline{W}$	Mixture molecular weight [kg/kmol]
λ	Mixture thermal conductivity [W/m/K]
$\hat{\rho}_{mem}$	Molar density of the membrane [kmol/m^3]
$\hat{h}_k$	Molar enthalpy of species *k* [J/kmol]

C_k	Molar fraction of bulk species *k*
$\dot{\omega}_k$	Molar production rate of gas-phase species *k* through homogeneous chemistry [kmol/m^3/s]
$\dot{s}_k$	Molar surface production rate of species *k* through heterogeneous chemistry [kmol/m^2/s]
W_k	Molecular weight of gas-phase species *k* [kg/kmol]
N_b	Number of bulk species
N_g	Number of gas-phase species
N_R	Number of surface reactions
N_s	Number of surface species
$V_O^{\bullet\bullet}$	Oxygen vacancy
A	Pre-exponential factor
k_i	Reaction rate constants of reaction *i*
$\dot{R}_i$	Reaction rate of reaction *i* [kmol/m^2/s]
σ	Stefan-Boltzmann constant [W/m^2/K^4]
$\nu_{k,i}$	Stoichiometric coefficient of species *k* in reaction *i*
Z_k	Surface site occupancy of surface species *k*
n	Temperature exponent
D_k^T	Thermal diffusion (Soret effect) coefficient [kg/m/s];
Γ	Total available surface site density [kmol/m^2]
R	Universal gas constant [J/mol/K]
(s)	Vacant surface site

subscripts

air	Air (feed) side of membrane
b	Backward reaction
f	Forward reaction

mem	Membrane
∞	Surrounding walls
sweep	Sweep gas (permeate) side of membrane

8. REFERENCES

1. J. Sunarso, S. Baumann, J.M. Serra, W.A. Meulenberg, S. Liu, Y.S. Lin, J.C. Diniz da Costa, *Mixed ionic-electronic conducting (MIEC) ceramic-based membranes for oxygen separation,* Journal of Membrane Science, **320** (1-2) (2008) 13-41.
2. J.G. McCarty, H. Wise, *Perovskite catalysts for methane combustion,* Catalysis Today, **8** (2) (1990) 231-248.
3. Y.S. Lin, Y. Zeng, *Catalytic properties of oxygen semipermeable perovskite-type ceramic membrane materials for oxidative coupling of methane,* Journal of Catalysis, **164** (1) (1996) 220-231.
4. Y. Liu, X. Tan, K. Li, *Mixed conducting ceramics for catalytic membrane processing,* Catalysis Reviews, **48** (2) (2006) 145-198.
5. Y. Zeng, Y.S. Lin, S.L. Swartz, *Perovskite-type ceramic membrane: synthesis, oxygen permeation and membrane reactor performance for oxidative coupling of methane,* Journal of Membrane Science, **150** (1) (1998) 87-98.
6. S.J. Xu, W.J. Thomson, *Perovskite-type oxide membranes for the oxidative coupling of methane,* AIChE Journal, **43** (11A) (1997) 2731-2740.
7. J.E. ten Elshof, H.J.M. Bouwmeester, H. Verweij, *Oxidative coupling of methane in a mixed-conducting perovskite membrane reactor,* Applied Catalysis A: General, **130** (2) (1995) 195-212.
8. X. Tan, Z. Pang, Z. Gu, S. Liu, *Catalytic perovskite hollow fibre membrane reactors for methane oxidative coupling,* Journal of Membrane Science, **302** (1-2) (2007) 109-114.
9. W. Jin, S. Li, P. Huang, N. Xu, J. Shi, Y.S. Lin, *Tubular lanthanum cobaltite perovskite-type membrane reactors for partial oxidation of methane to syngas,* Journal of Membrane Science, **166** (1) (2000) 13-22.
10. U. Balachandran, J.T. Dusek, R.L. Mieville, R.B. Poeppel, M.S. Kleefisch, S. Pei, T.P. Kobylinski, C.A. Udovich, A.C. Bose, *Dense ceramic membranes for partial oxidation of methane to syngas,* Applied Catalysis A: General, **133** (1) (1995) 19-29.
11. H.J.M. Bouwmeester, *Dense ceramic membranes for methane conversion,* Catalysis Today, **82** (1-4) (2003) 141-150.
12. X. Tan, K. Li, A. Thursfield, I.S. Metcalfe, *Oxyfuel combustion using a catalytic ceramic membrane reactor,* Catalysis Today, **131** (1-4) (2008) 292-304.
13. J. Hong, P. Kirchen, A.F. Ghoniem, *Interactions between oxygen permeation and homogeneous-phase fuel conversion on the sweep side of an ion transport membrane,* Journal of Membrane Science, **428** (2013) 309-322.
14. F.T. Akin, J.Y.S. Lin, *Oxygen permeation through oxygen ionic or mixed-conducting ceramic membranes with chemical reactions,* Journal of Membrane Science, **231** (1-2) (2004) 133-146.
15. Z. Rui, Y. Li, Y.S. Lin, *Analysis of oxygen permeation through dense ceramic membranes with chemical reactions of finite rate,* Chemical Engineering Science, **64** (1) (2009) 172-179.
16. W. Wang, Y.S. Lin, *Analysis of oxidative coupling of methane in dense oxide membrane reactors,* Journal of Membrane Science, **103** (3) (1995) 219-233.
17. Z. Rui, K. Zhang, Y. Li, Y.S. Lin, *Simulation of methane conversion to syngas in a membrane reactor: Part I A model including product oxidation,* International Journal of Hydrogen Energy, **33** (9) (2008) 2246-2253.
18. Z. Rui, K. Zhang, Y. Li, Y.S. Lin, *Simulation of methane conversion to syngas in a membrane reactor. Part II Model predictions,* International Journal of Hydrogen Energy, **33** (10) (2008) 2501-2506.
19. W. Jin, X. Gu, S. Li, P. Huang, N. Xu, J. Shi, *Experimental and simulation study on a catalyst packed tubular dense membrane reactor for partial oxidation of methane to syngas,* Chemical Engineering Science, **55** (14) (2000) 2617-2625.
20. X. Tan, K. Li, *Design of mixed conducting ceramic membranes/reactors for the partial oxidation of methane to syngas,* AIChE Journal, **55** (10) (2009) 2675-2685.
21. J. Hong, P. Kirchen, A.F. Ghoniem, *Numerical simulation of ion transport membrane reactors: oxygen permeation and transport and fuel conversion,* Journal of Membrane Science, **407-408** (2012) 71-85.

22. J. Hong, P. Kirchen, A.F. Ghoniem, *Laminar oxy-fuel diffusion flame supported by an oxygen-permeable-ion-transport membrane,* Combustion and Flame, **160** (3) (2013) 704-717.
23. S.J. Xu, W.J. Thomson, *Oxygen permeation rates through ion-conducting perovskite membranes,* Chemical Engineering Science, **54** (17) (1999) 3839-3850.
24. J.E. ten Elshof, H.J.M. Bouwmeester, H. Verweij, *Oxygen transport through $La_{1-x}Sr_xFeO_{3-\delta}$ membranes* ||. *Permeation in air/CO, CO_2 gradients,* Solid State Ionics, **89** (1-2) (1996) 81-92.
25. X. Tan, L. Shi, G. Hao, B. Meng, S. Liu, *$La_{0.7}Sr_{0.3}FeO_{3-\alpha}$ perovskite hollow fiber membranes for oxygen permeation and methane conversion,* Separation and Purification Technology, **96** (2012) 89-97.
26. G.P. Smith, D.M. Golden, M. Frenklach, N.W. Moriarty, B. Eiteneer, M. Goldenberg, C.T. Bowman, R.K. Hanson, S. Song, W.C. Gardiner, V.V. Lissianski, Z. Qin. *GRI-Mech 3.0*. Available from: http://www.me.berkeley.edu/gri_mech/.
27. D.G. Goodwin. *Cantera*. Available from: http://www.aresinstitute.org/Cantera/cantera-cxx.pdf.
28. O. Deutschmann, R. Schmidt, F. Behrendt, J. Warnat, *Numerical modeling of catalytic ignition,* Symposium (International) on Combustion, **26** (1) (1996) 1747-1754.
29. L.L. Raja, R.J. Kee, L.R. Petzold, *Simulation of the transient, compressible, gas-dynamic behavior of catalytic-combustion ignition in stagnation flows,* Symposium (International) on Combustion, **27** (2) (1998) 2249-2257.
30. D.G. Goodwin, H. Zhu, A.M. Colclasure, R.J. Kee, *Modeling electrochemical oxidation of hydrogen on Ni-YSZ pattern anodes,* Journal of the Electrochemical Society, **156** (9) (2009) B1004-B1021.
31. J. Fleig, *On the current-voltage characteristics of charge transfer reactions at mixed conducting electrodes on solid electrolytes,* Phys. Chem. Chem. Phys., **7** (9) (2005) 2027-2037.
32. B.A. Boukamp, K.J. de Vries, A.J. Burggraaf, *Surface oxygen exchange in bismuth oxide based materials*. Non-stoichiometric compounds: surfaces, grain boundaries and structural defects, ed. J. Nowotny and W. Weppner, Kluwer, 1989.
33. B.A. Boukamp, H. Verweij, A.J. Burggraaf, *Solid State Ionics* |||, ed. G.A. Nazri, J.M. Tarascon, and M. Armand, Materials Research Society, 1993.
34. E.S. Hecht, G.K. Gupta, H. Zhu, A.M. Dean, R.J. Kee, L. Maier, O. Deutschmann, *Methane reforming kinetics within a Ni-YSZ SOFC anode support,* Applied Catalysis A: General, **295** (1) (2005) 40-51.
35. V.M. Janardhanan, O. Deutschmann, *CFD analysis of a solid oxide fuel cell with internal reforming: Coupled interactions of transport, heterogeneous catalysis and electrochemical processes,* Journal of Power Sources, **162** (2) (2006) 1192-1202.
36. H.J.M. Bouwmeester, C. Song, J. Zhu, J. Yi, M. van Sint Annaland, B.A. Boukamp, *A novel pulse isotopic exchange technique for rapid determination of the oxygen surface exchange rate of oxide ion conductors,* Phys. Chem. Chem. Phys., **11** (42) (2009) 9640-9643.
37. B.A. van Hassel, J.E. ten Elshof, H.J.M. Bouwmeester, *Oxygen permeation flux through $La_{1-y}Sr_yFeO_3$ limited by carbon monoxide oxidation rate,* Applied Catalysis A: General, **119** (2) (1994) 279-291.
38. P. Kirchen, D. Apo, A. Hunt, A.F. Ghoniem, *A novel ion transport membrane reactor for fundamental investigations of oxygen permeation and oxy-combustion under reactive flow conditions,* Proceedings of the Combustion Institute, **34** (2) (2013) 3463-3470.

List of Figures

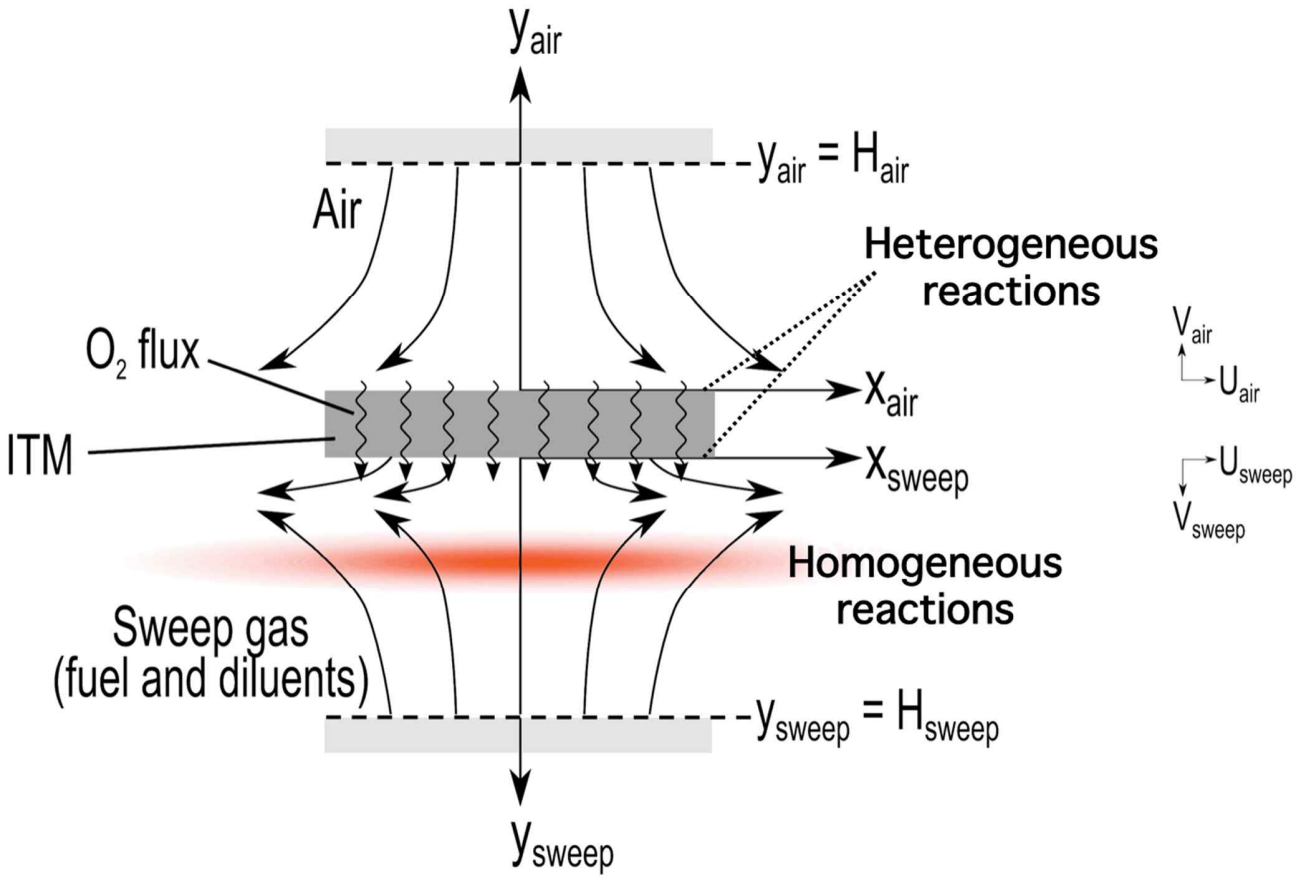

Figure 1 Planar, finite-gap stagnation flow configuration considered in this study (revised from [22]), where H_{air} = air channel height and H_{sweep} = sweep gas channel height. $y_{air} = 0$ and $y_{sweep} = 0$ are located on the membrane surfaces of the air and sweep side, respectively.

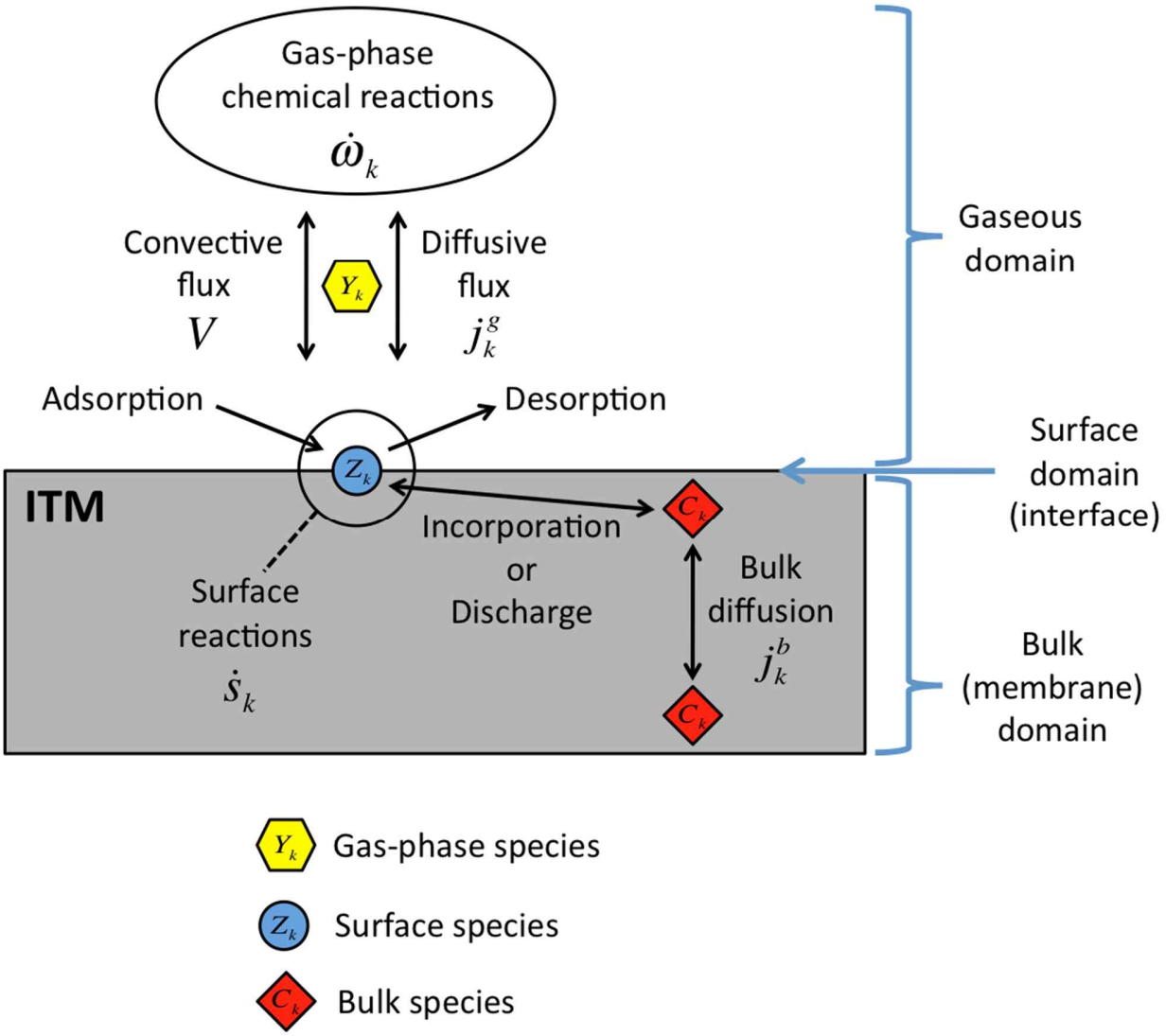

Figure 2 Three domains (i.e., gaseous, surface and bulk domains) and the species belonging to each domain (i.e., Y_k = gas-phase species in the gaseous domain, Z_k = surface species in the surface domain and C_k = bulk species in the bulk domain) considered in this study. The gaseous and bulk domains are volumetric domains, whereas the surface domain is an interface domain between these two volumetric domains

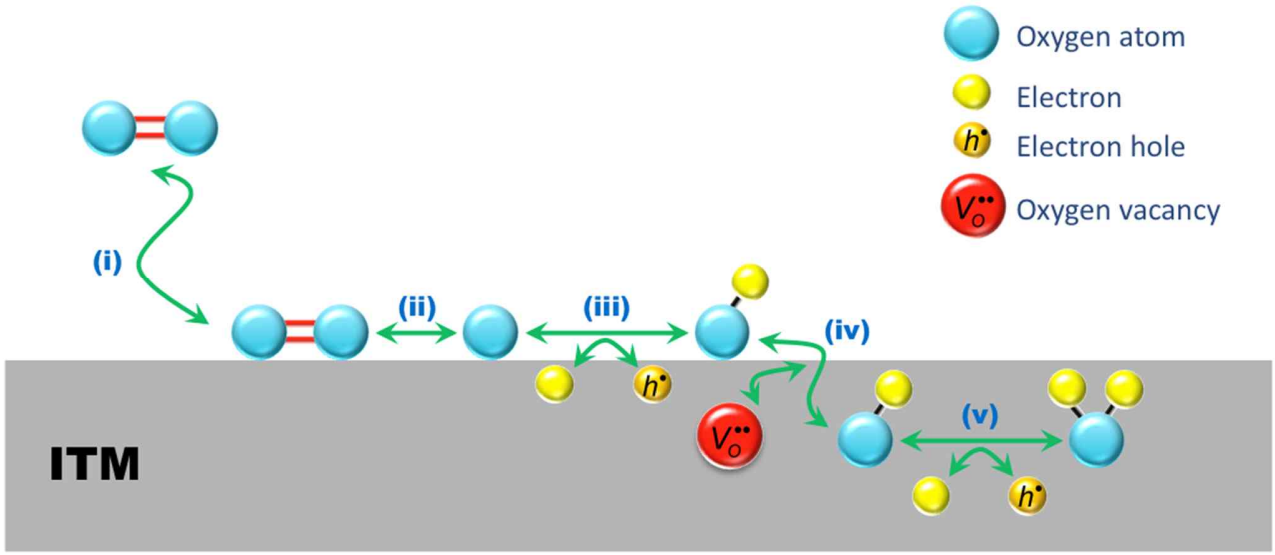

Figure 3 Five intermediate steps for the oxygen surface exchange process. The step (i) to (iii) corresponds to dissociative/associative adsorption/desorption (surface reaction 1, Eq.12), and the step (iv) to (v) refers to charge-transfer incorporation/discharge (surface reaction 2, Eq.13)

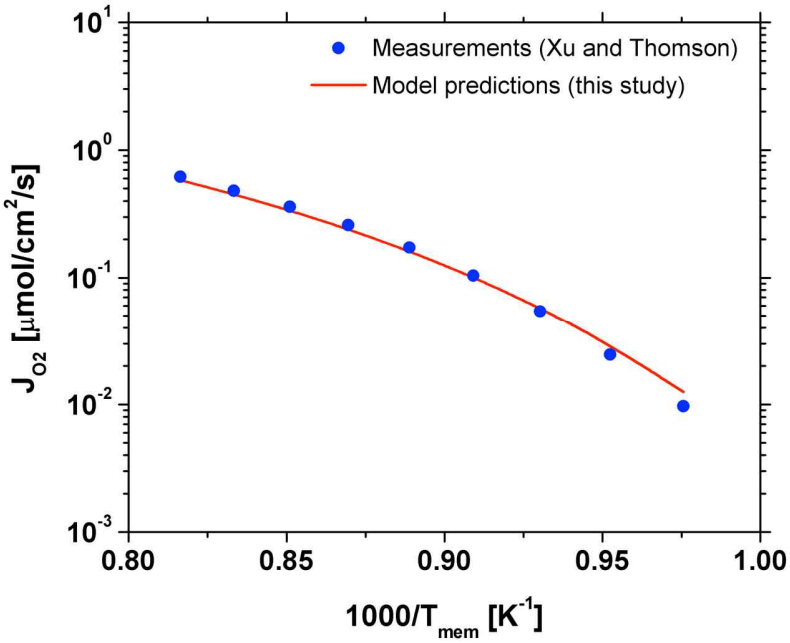

(a)

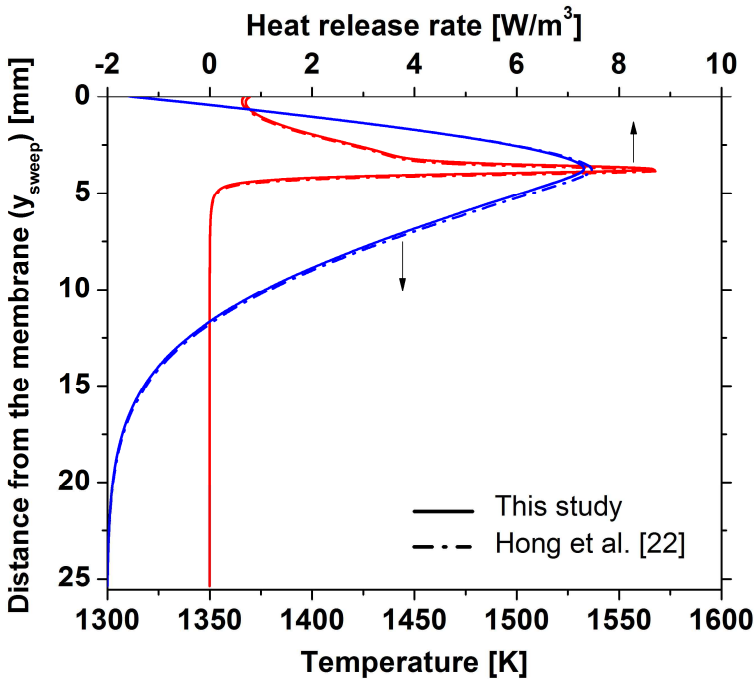

(b)

Figure 4 (a) Comparison between the oxygen permeation rates estimated using the oxygen surface exchange kinetic parameters obtained in this study and those measured by Xu and Thomson [23] and (b) comparison between the heat release rate and temperature evaluated using the oxygen surface exchange kinetic parameters obtained in this study and those estimated by Hong et al. [22]

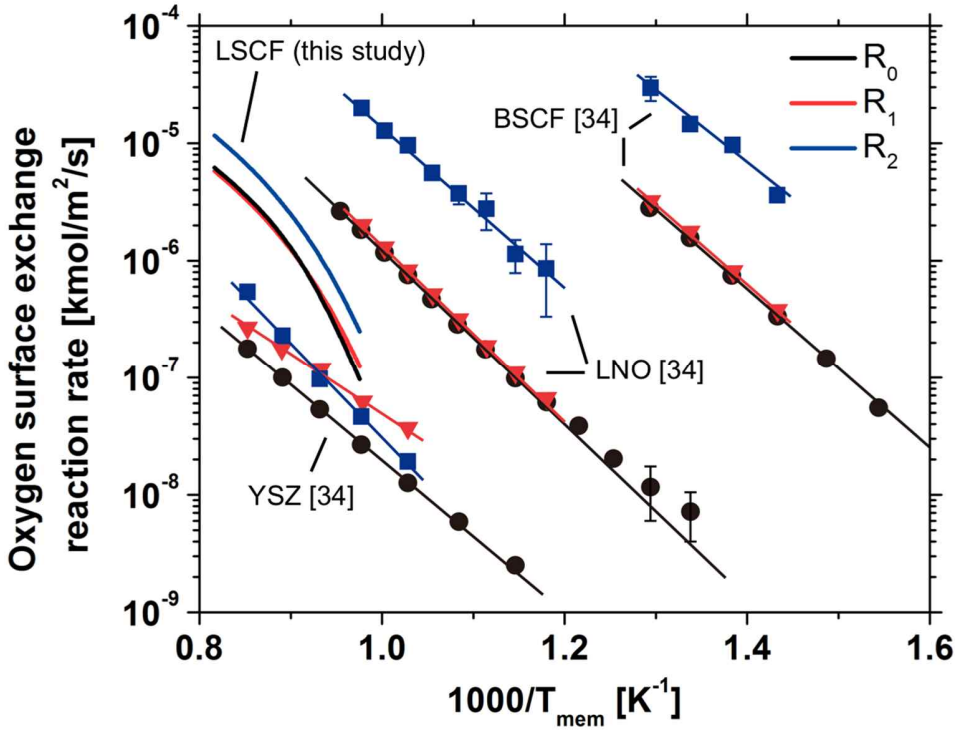

Figure 5 The oxygen surface exchange reaction rates for LSCF estimated by the model. Experimentally determined exchange rates for YSZ, LNO and BSCF [36]. R_0 is the global surface exchange reaction rate for Eq.11, while R_1 and R_2 corresponds to Eq.15 and Eq.16 for the two rate-limiting reactions.

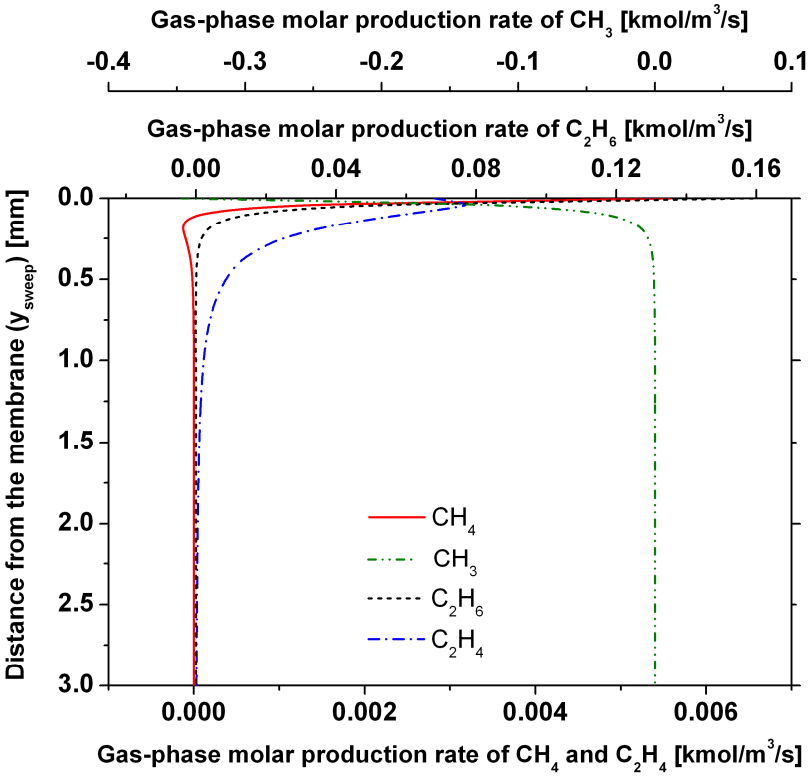

Figure 6 The molar production rate of CH_4, CH_3, C_2H_6 and C_2H_4 from the homogeneous-phase reactions as predicted by the model, given the sweep side conditions considered in experiments performed by Xu and Thomson [6]. The surface molar production rate of CH_4 is −1.02 kmol/m^2/s, while that of CH_3 is 1.02 kmol/m^2/s.

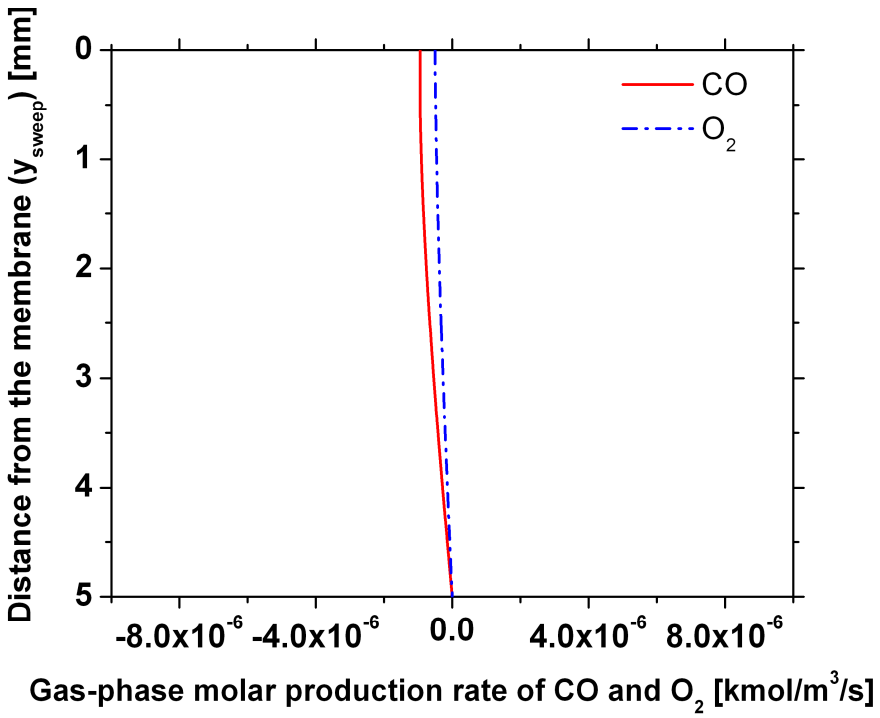

Figure 7 The molar production rate of CO and O_2 from the homogeneous-phase reactions as predicted by the model, given the sweep side conditions considered in experiments performed by ten Elshof et al. [24]. The surface molar production rate of CO is −5.51 kmol/m^2/s.

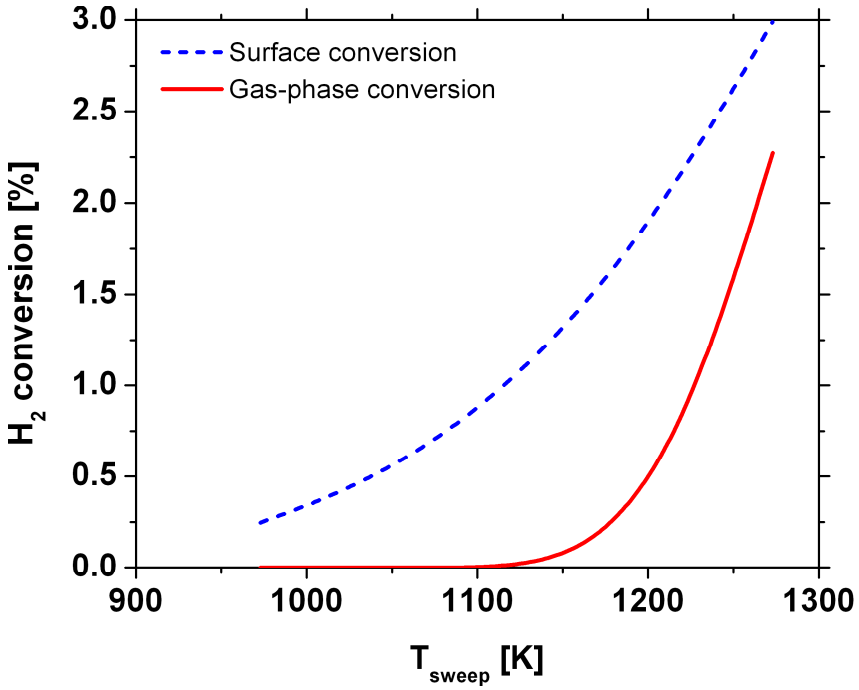

Figure 8 Contribution of the catalytic surface reactions and the homogeneous-phase reactions to hydrogen oxidation as predicted by the model, given the sweep side conditions considered in experiments performed by Tan et al. [25]

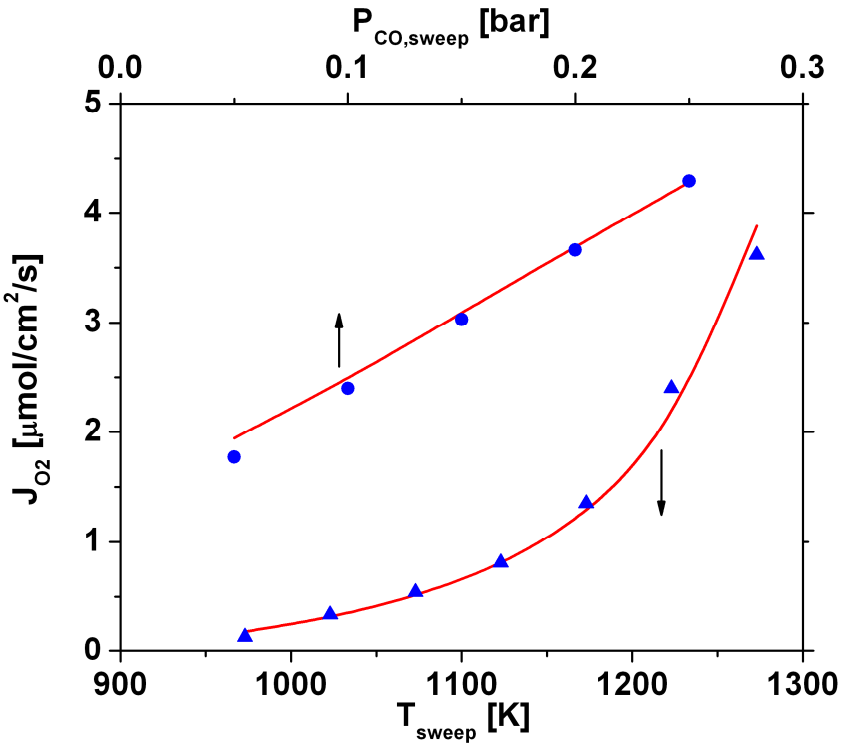

Figure 9 The oxygen permeation rate estimated using the catalytic fuel conversion kinetic parameters obtained in this study and those measured by ten Elshof et al. [24] and Tan et al. [25]

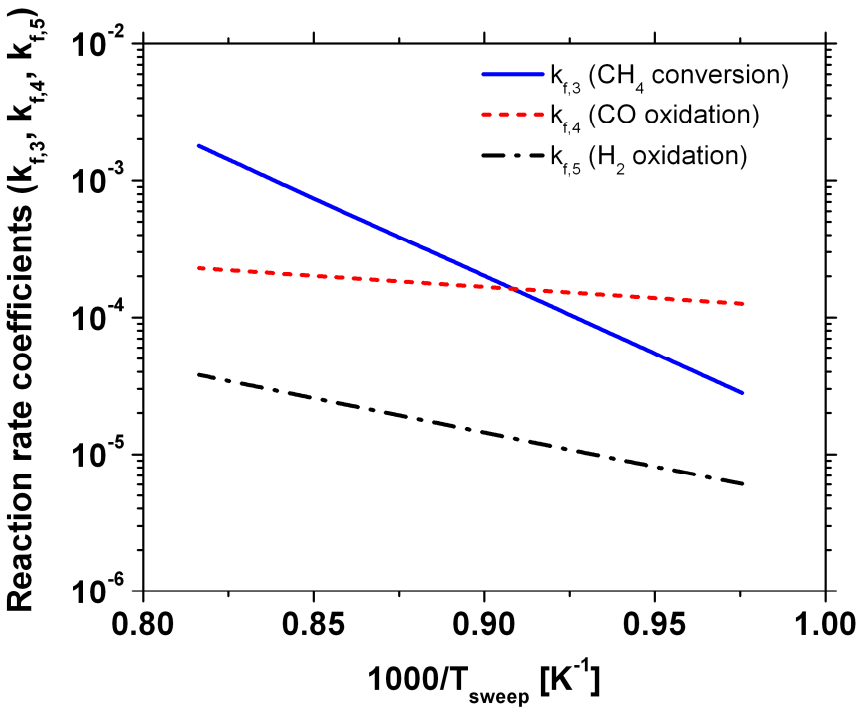

Figure 10 The kinetic parameters for catalytic fuel conversion estimated using the model ($k_{f,3}$ = CH_4 catalytic decomposition reaction rate constant, $k_{f,4}$ = CO surface oxidation reaction rate constant, $k_{f,5}$ = H_2 surface oxidation reaction rate constant)

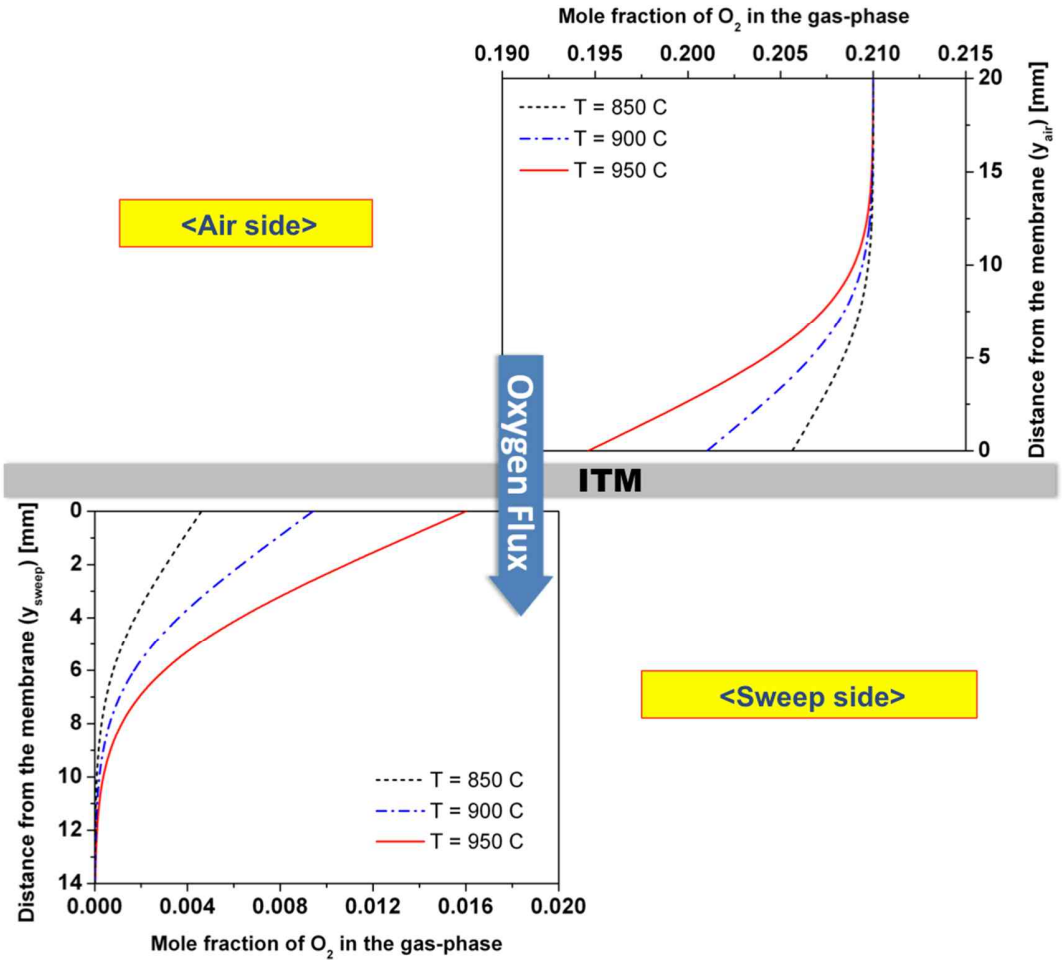

Figure 11 The spatially resolved gas-phase oxygen concentration in both sides of the membrane, given the air and sweep gas conditions considered in the estimation of the kinetic parameters for the oxygen surface exchange reactions

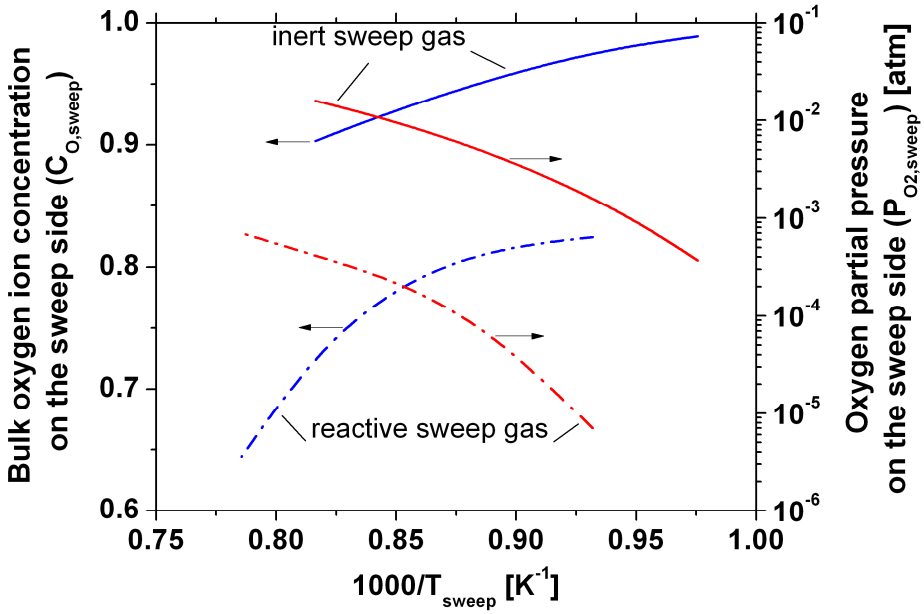

Figure 12 The bulk oxygen ion concentration and the oxygen partial pressure in the immediate vicinity of the membrane on the sweep side evaluated using the model given the sweep gas inlet conditions when an inert sweep gas [23] or a reactive sweep gas [25] is introduced

List of Tables

Table 1 The oxygen surface exchange kinetic parameters for the two rate-limiting reactions and the catalytic fuel conversion kinetic parameters for CH_4, CO and H_2 oxidation (the units of the pre-exponential factor, A, are in kmol, m^3, second)

Reaction number	Reactions	Reaction rate constants	Pre-exponential factor, A	Temperature exponent, n	Activation energy, E_A [J/mol]
Oxygen surface exchange kinetics					
1	$O_2 + 2(s) \leftrightarrow 2O^-(s)$	$k_{f,1}$	1.00 E+30	0	2.68 E+05
		$k_{b,1}$	2.30 E+27	3.6	3.15 E+05
2	$O^-(s) + V_O^{\bullet\bullet} \leftrightarrow O_O^x + (s)$	$k_{f,2}$	1.20 E+13	5.2	3.66 E+05
		$k_{b,2}$	3.30 E+07	5.2	4.35 E+05
Catalytic fuel conversion kinetics					
3	$2CH_4 + O_O^x \rightarrow 2CH_3 + H_2O + V_O^{\bullet\bullet}$	$k_{f,3}$	3.20 E+14	0	2.17 E+05
4	$CO + O_O^x \rightarrow CO_2 + V_O^{\bullet\bullet}$	$k_{f,4}$	4.79 E+02	0	3.10 E+04
5	$H_2 + O_O^x \rightarrow H_2O + V_O^{\bullet\bullet}$	$k_{f,5}$	1.10 E+02	0.75	8.86 E+04